nature ecology & evolution

ARTICLES

https://doi.org/10.1038/s41559-018-0759-0

Global plant–symbiont organization and emergence of biogeochemical cycles resolved by evolution-based trait modelling

Mingzhen Lu* and Lars O. Hedin

One of the most distinct but unresolved global patterns is the apparent variation in plant–symbiont nutrient strategies across biomes. This pattern is central to our understanding of plant–soil–nutrient feedbacks in the land biosphere, which, in turn, are essential for our ability to predict the future dynamics of the Earth system. Here, we present an evolution-based trait-modelling approach for resolving (1) the organization of plant–symbiont relationships across biomes worldwide and (2) the emergent consequences for plant community composition and land biogeochemical cycles. Using game theory, we allow plants to use different belowground strategies to acquire nutrients and compete within local plant–soil–nutrient cycles in boreal, temperate and tropical biomes. The evolutionarily stable strategies that emerge from this analysis allow us to predict the distribution of belowground symbioses worldwide, the sequence and timing of plant succession, the bistability of ecto- versus arbuscular mycorrhizae in temperate and tropical forests, and major differences in the land carbon and nutrient cycles across biomes. Our findings imply that belowground symbioses have been central to the evolutionary assembly of plant communities and plant–nutrient feedbacks at the scale of land biomes. We conclude that complex global patterns emerge from local between-organism interactions in the context of Darwinian natural selection and evolution, and that the underlying dynamics can be mechanistically probed by our low-dimensional modelling approach.

Belowground plant symbioses have been central to the evolution and distribution of vascular plants in the land biosphere[1–4], with potentially far-reaching effects on ecosystem nutrient cycles and the land carbon sink[5–10]. Yet, it has been difficult to capture the emergence of global patterns in symbioses and nutrient cycles using first-principle ecological theories. A major obstacle has been the problem of characterizing how the fundamental biology of plant symbioses interacts with the processes of plant–plant competition and community assembly. Here, we present a new approach that—despite a simple mathematical structure—is capable of resolving the complex organization of plant–symbiont strategies and nutrient cycles at the scale of biomes.

Central to our approach is the observation that plants have evolved functionally different strategies to trade photosynthetically acquired carbon to compete for limiting soil nutrients: (1) by scavenging[11] plant-available nutrients (for example, nitrates, phosphates and amino acids) in symbiosis with arbuscular mycorrhizal fungi (AMF; the scavenger strategy); (2) by mining[12,13] organic-bound nutrients in symbiosis with ecto- and ericoid mycorrhizal fungi (hereafter combined as EMF; the miner strategy; Methods); or (3) by acquiring atmospheric nitrogen in symbiosis with nitrogen-fixing bacteria[5,14] (NFB; the fixer strategy). Plant roots that have no symbiotic associations (naked roots) rely solely on their absorptive surface for uptake of available nutrients.

The evolution of these plant–symbiont relationships (Fig. 1) has fundamentally advanced the ability of plants to overcome nutrient limitation, impact biogeochemical cycles and perhaps also expand into inhospitable geographical regions[15]. The scavenger strategy is the earliest-evolved symbiosis[16,17] (AMF: ~400 million years ago (Ma)), the miner strategy is secondarily evolved[16,18] (EMF: ectomycorrhizae ~200 Ma; ericoid mycorrhizae ~100 Ma) and the nitrogen fixer strategy is most recently evolved[19] (NFB: ~60 Ma).

Here, we investigate how these innovations of plant–symbiont strategies have influenced (or been influenced by) biogeochemical cycles at scales of biomes. Specifically, we use an evolution-based approach to evaluate the mutation and selection of traits that define each plant symbiotic strategy, and its broader impact on nutrient cycles.

We present a modelling approach (Box 1) that allows plant–symbiont strategies to evolve in the context of: (1) local plant–plant competition for limiting soil nitrogen or phosphorus; (2) an explicit carbon cost trade-off for each symbiotic strategy; and (3) a dynamical plant–soil–nutrient feedback. We treat each symbiotic strategy as a collection of traits that are subject to incremental mutation. We explore the full trait space that makes up each strategy, and search for the emergence of evolutionarily stable strategies (ESSs) within each community. ESSs are defined as strategies that cannot be invaded by any other mutant strategy in a given local community.

Our approach is inherently low dimensional, based on three fundamental equations and four biome-scale assumptions. The three equations (Box 1 and Methods) track plant biomass, soil organic matter, and plant-available nutrients. We assume that biomes differ only in four variables (Table 1a). First, maximum gross primary production (G), soil decomposition (m), and forest disturbance (d) all decrease from tropical to temperate, and to boreal forest. Second, land surfaces that were glaciated in the Last Glacial Maximum carry larger quantities of soil phosphorus, causing higher weathering input of plant-available phosphorus.

Moreover, our approach differs from models that seek to optimize biological properties such as primary productivity or biomass at the ecosystem level. Instead, we allow the most successful individual plant strategies to emerge within the plant–nutrient cycle created by the collective plant community—regardless of whether the emergent properties are optimal at the ecosystem scale.

Department of Ecology and Evolutionary Biology, Princeton University, Princeton, NJ, USA. *e-mail: mingzhen@princeton.edu

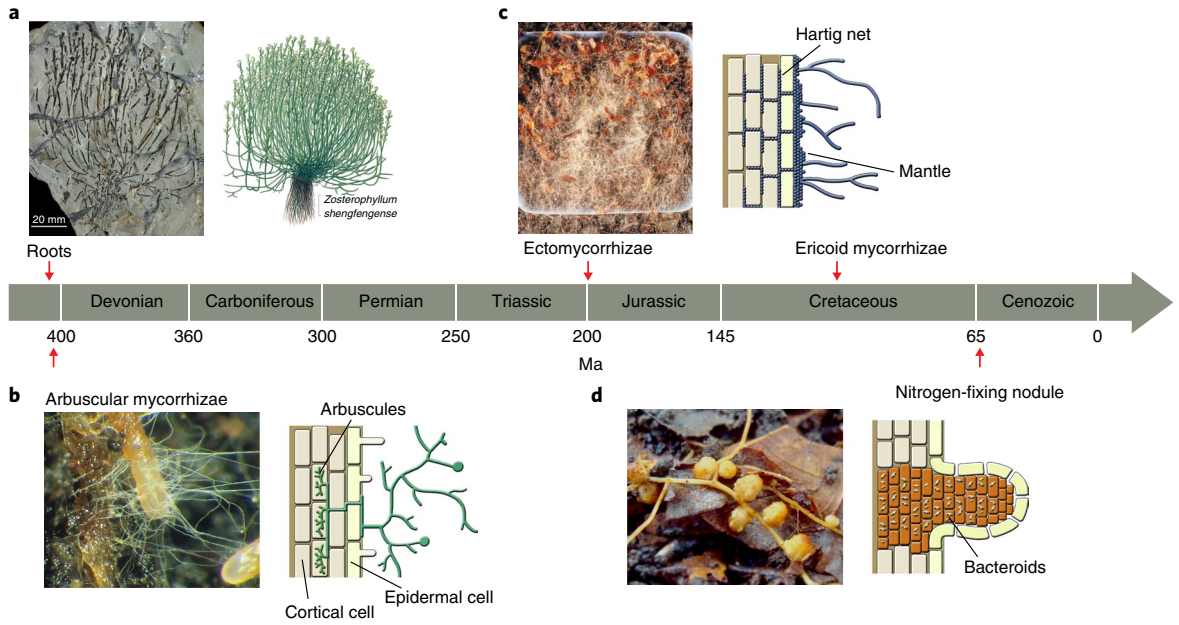

Fig. 1 | Timeline of the plant–symbiont relationship on land. a, Earliest fossil record (413 Ma; left) and schematic (right) of a true rooting system from the Early Devonian plant *Zosterophyllum shengfengense*[69], indicating that land plants had developed roots capable of resource uptake. **b**, AMF-like fungal root structures were found early in the fossil record (~407 Ma[70]), aiding plants in acquiring soil resources. Left, image of a fine root colonized by AMF fungi. Right, schematic of how root-colonizing AMF hyphae (green) extend the absorptive area of roots (adapted from ref. [71]). Epidermal cells are light yellow and cortical cells are light brown in all schematics. **c**, Ectomycorrhizal fungi evolved from their wood-decaying ancestors ~200 Ma[16], with the unique capability of producing hydrolytic and oxidative extracellular enzymes that help plants access organic-bound nutrients. Left, EMF fungi (white furry strands) feeding on *Fagus* litter[38]. Right, schematic of how EMF hyphae (purple) form two structures: a thick mantle on the root surface and a Hartig net beneath the epidermal cells. **d**, The innovation of symbiotic nitrogen fixation emerged ~50–60 Ma, allowing plants a unique but costly mechanism for overcoming nitrogen limitation[19]. Left, *Inga punctata* roots and nodules in a Panamanian tropical forest. Right, schematic of root nodule cells (orange, derived from cortical cells) containing symbiotic nitrogen-fixing *Rhizobia* bacteria. Each bacterial cell is encapsulated by a plant intercellular membrane in a bacteroid structure. Image credits: **a**, Jinzhuang Xue; **b**, Paula Flynn; **c**, David Read; **d**, Sarah Batterman. Illustration in **a**, J. Xue; illustrations in **b**–**d**, Y. Sun.

Results and discussion

Global pattern of the plant–symbiont relationship. Read[1], Jenny[20] and others[5,6,10] have suggested that the geographical distribution of root symbioses may vary systematically across biomes. We compiled a global dataset of belowground plant strategies by combining Gentry's quantitative vegetation survey of 225 sites worldwide (Fig. 2a) with a new taxon-specific database on root symbioses that we developed from the literature (Methods).

Our results confirm the following global trends (Fig. 2b–d): (1) the AMF symbiosis dominates the tropical forest biome and is common in temperate forests; (2) EMF dominates the boreal biome, is common in temperate forests and can form dominant patches in tropical forests (for example, South America[13], Central Africa[21] or widespread dipterocarp forests in Southeast Asia[22]; red points in Fig. 2a,c); and (3) NFB is common in early- and late-successional tropical forests, but limited to early succession in temperate and boreal biomes[5,10]. Moreover, nitrogen-fixing trees appear to employ a facultative fixation strategy[23,24] in tropical forests, but an obligate[25] strategy in temperate and boreal biomes.

Biome-level prediction of symbiotic composition. Most notably, our ESS model can recreate the observed global patterns of plant–symbiont relationships. We made predictions of tree community composition across biomes (Fig. 3a) by combining our community-level ESS analysis with observed rates of forest disturbance[26]: low in boreal ($d = 1/100\,\mathrm{yr}^{-1}$), medium in temperate ($1/70\,\mathrm{yr}^{-1}$) and high in tropical forests ($1/50\,\mathrm{yr}^{-1}$). For each biome, we seeded a landscape (Fig. 3b) with either the community-level ESS or the best-performing mutant strategy in cases of no community-level ESS, and allowed them to interact and self-assemble. Each landscape patch was subject to stochastic disturbance at the biome-specific rate (Methods), which, over time, generated a mosaic of soil conditions and forest successional stages.

The predictions from our model (Fig. 3a) are broadly consistent with the biome patterns in Fig. 2: EMF dominated the boreal and glaciated temperate biome, coexisting with a small component of obligate fixers. In contrast, AMF dominated the tropical biome with relatively abundant (~10% of biomass) facultative fixers. Non-glaciated temperate forests displayed a transitional condition, with AMF and EMF coexisting, and with low abundances of obligate fixers.

Nutrient limitation and forest succession. These model predictions translated into distinct patterns of nutrient limitation on plant growth across biomes. We show in Fig. 3 the distribution of nutrient limitation within each biome landscape, with each patch characterized by a unique limitation status (Methods). As is generally inferred from fertilization experiments[27], we found the boreal biome to be exclusively limited by nitrogen and the tropical forest to be predominantly limited by phosphorus (Fig. 3c–f). The temperate biome occupies an intermediate state, with glaciated areas most frequently limited by nitrogen and non-glaciated areas by either nitrogen or phosphorus (Fig. 3d,e).

Succession plays an important role in generating the patterns of plant community composition (Fig. 3a) and nutrient limitation (Fig. 3c–f) that emerge within our model. Our model prediction agrees with the empirically observed[7,10,25] sequence and timing of succession of belowground strategies across biomes (Supplementary Fig. 2a–c): in boreal and temperate forests, obligate NFB trees

Box 1 | Evolution-based trait model

Model structure. Our model considers key components of the forest carbon and nutrient cycles, nutrient limitation on plant growth and, crucially, that plants can trade photosynthetically acquired carbon to gain nutrients from belowground symbionts. We consider nitrogen and phosphorus as they often constrain plant growth, but our model can, in principle, be adapted to any potentially limiting macro- or micronutrient. Three fundamental equations track carbon and nutrient cycling between plant biomass (B; equation (1)), organic-bound soil nutrients (O_i; equation (2), Methods) and plant-available forms of soil nutrients (A_i; equation (3), Methods), where i=N denotes nitrogen and i=P denotes phosphorus. Net plant biomass growth (change of biomass through time t) is limited by either nutrient assimilation (g_i) or photosynthetic carbon gain (g_C):

$$\frac{dB}{dt} = (\min(g_C, g_N, g_P) - \mu - d_j)B \quad (1)$$

where μ is plant biomass turnover owing to tissue mortality and d_j is the biome-specific (subscript j) disturbance rate imposed by external forces, including wind-throw, landslides, fire, and so on.

Carbon-based growth in equation (1) is defined as the balance between gross photosynthesis, plant tissue respiration (δ) and the costs incurred by belowground nutrient acquisition (θ_X, where X denotes the form of the plant–symbiont relationship):

$$g_C = \frac{\alpha G_j}{\alpha B + c_G} - \delta - (1-\alpha)(\theta_S S + \theta_M M + (\theta_F + \psi)F + \theta_v v(X)) \quad (1a)$$

Photosynthesis saturates as a function of aboveground biomass (αB) with a biome-specific maximum gross photosynthesis rate (G_j) and the half-saturation constant c_G. Plants pay a metabolic carbon cost for acquiring a nutrient by scavenging (θ_S), mining (θ_M), fixation (θ_F) and naked root uptake (θ_v), and an opportunistic cost[5] for maintaining a root system that supports the facultative fixation strategy (ψ).

Nutrient-based growth in equation (1) is defined as the product of the plant nutrient-use efficiency (ω_i) and the nutrient assimilated by the rooting system, where $1-\alpha$ is the root fraction of plant biomass:

$$g_i = \omega_i(1-\alpha)\left(\frac{S_i A_i}{A_i + c_i^S} + \frac{M_i O_i}{O_i + c_i^M} + F_N + \frac{v_i(X)A_i}{A_i + c_i^v}\right) \quad (1b)$$

The first uptake term in equation (1b) demonstrates that nutrient assimilation by the scavenger strategy (S) is a saturating function of A_i with per-root biomass uptake rate S_i and half-saturation constant c_i^S. In the second term, the miner strategy (M) acquires organic-bound nutrients (O_i) at the rate M_i and half-saturation constant c_i^M. In the third term, the fixer strategy (F) can acquire nitrogen at the rate F_N and employ either an obligate or facultative fixation strategy[5] (Methods). As observed in nature[74], fixers can associate with either AMF or EMF fungi, such that each fixer genotype is defined by a specific fixation rate and either a miner or scavenger rate. Finally, the fourth term defines nutrient uptake by the naked root at the rate v and half-saturation constant c_i^v, and the dependence of v on symbiont colonization X (described below). As demonstrated empirically[11], we consider that naked roots have a high half-saturation constant (that is, high c_i) consistent with low affinity for available nutrients (the model parameters are summarized in Supplementary Table 1).

We scaled biomass abundances of phosphorus versus nitrogen to approximate the stoichiometric ratio observed in living and dead organic matter (~1:10)[75,76]. We also considered the observation that AMF fungi appear to be superior at acquiring soil phosphorus[11]. As a result, we reduced the carbon cost of phosphorus uptake (relative to nitrogen uptake) for the scavenger strategy, such that the stoichiometric ratio of phosphorus versus nitrogen uptake per unit of carbon invested was higher for the scavenger (3:10) than the miner or naked root strategies (1:10).

Essential trade-offs. Our model captures two fundamental cost trade-offs that are critical to our ability to predict plant nutrient acquisition: a 'nutrient–carbon–growth trade-off' and/or a 'nutrient uptake trade-off'. By employing belowground symbionts, a plant can gain access to nutrients from sources that naked roots cannot exploit or at concentrations that are lower than those naked roots can consume. However, this action carries two costs: (1) the plant sacrifices photosynthetically acquired carbon that could otherwise be used for above- or belowground biomass growth (the nutrient–carbon–growth trade-off in equation (1a) and Supplementary Note 1); and (2) the plant sacrifices the ability to acquire nutrients through its own low-cost root surface since association with symbionts is known to physically interfere with the root area available for nutrient uptake (the nutrient uptake trade-off in Supplementary Note 3). Following ref. [5], we capture this trade-off by allowing naked root uptake to decease with increased symbiont colonization (equation (4), Methods).

Community-level ESS analyses. We allowed plants to vary their trait values (scavenger, miner or fixer) and assumed that these variations are genetically determined and subject to mutation. We then evaluated a mutant's competitive ability to invade a forest with a plant–soil–nutrient cycle established by a resident tree population.

Using pairwise invasibility analysis[5], we show in Supplementary Fig. 1a an example of competition between resident (x axis) and invader strategies (y axis) across AMF mutant genotypes in a temperate forest. The emergent ESS is the resident strategy that cannot be eliminated by any mutant (vertical red bar in Supplementary Fig. 1). We applied the ESS analysis to the entire plant community, by allowing pairwise competition across all mutants and all strategies (Supplementary Fig. 1b–g). The resulting community-level ESS (marked by a red star) identifies the specific strategies that can resist invasion from any other mutant of any strategy across the entire plant community.

First, we analysed mature forests with little to no external disturbance (d=0). EMF was the only community-level ESS in the boreal biome, where plant-available nitrogen was low, organic-bound nutrients ample and weatherable phosphorus abundant. In contrast, both AMF and EMF were possible community-level ESSs in tropical and temperate forests, independent of glacial history.

Second, we examined disturbed forests (d=1/20 yr^{-1}) characterized by open canopy and a shortage of available nutrients relative to plant demand (as observed in nature[25,77]). In these conditions, NFB was the sole community-level ESS across all biomes (Supplementary Fig. 1e–g), with obligate fixation dominating in nitrogen-poor extra-tropical forests, and facultative fixation in nitrogen-rich tropical forests (as observed in nature[10,25] and modelled previously[5]).

Biome-scale assumptions. To predict patterns observed in nature (later described in Fig. 2), we prescribed four empirically observed differences across boreal, temperate and tropical biomes (Table 1a): (1) climate and growing season length cause G_j to decrease with increasing latitude[45]; (2) temperature causes soil

Box 1 | (Continued)

nutrient mineralization (m_j; Methods) to decrease with increasing latitude[46,78]; (3) recent glacial history (that is, glacial grinding of primary rocks) causes the weathering input of soil phosphorus to increase (I_P; Methods) in boreal and high-latitude temperate biomes; and (4) meta-analyses have shown that d_j decreases with increasing latitude[26], possibly due to differences in soils and/or energetic conditions of the climate system[79]. As observed in nature, the temperate biome therefore contains both high-phosphorus glaciated and low-phosphorus non-glaciated soils; we treat these conditions separately in our analyses.

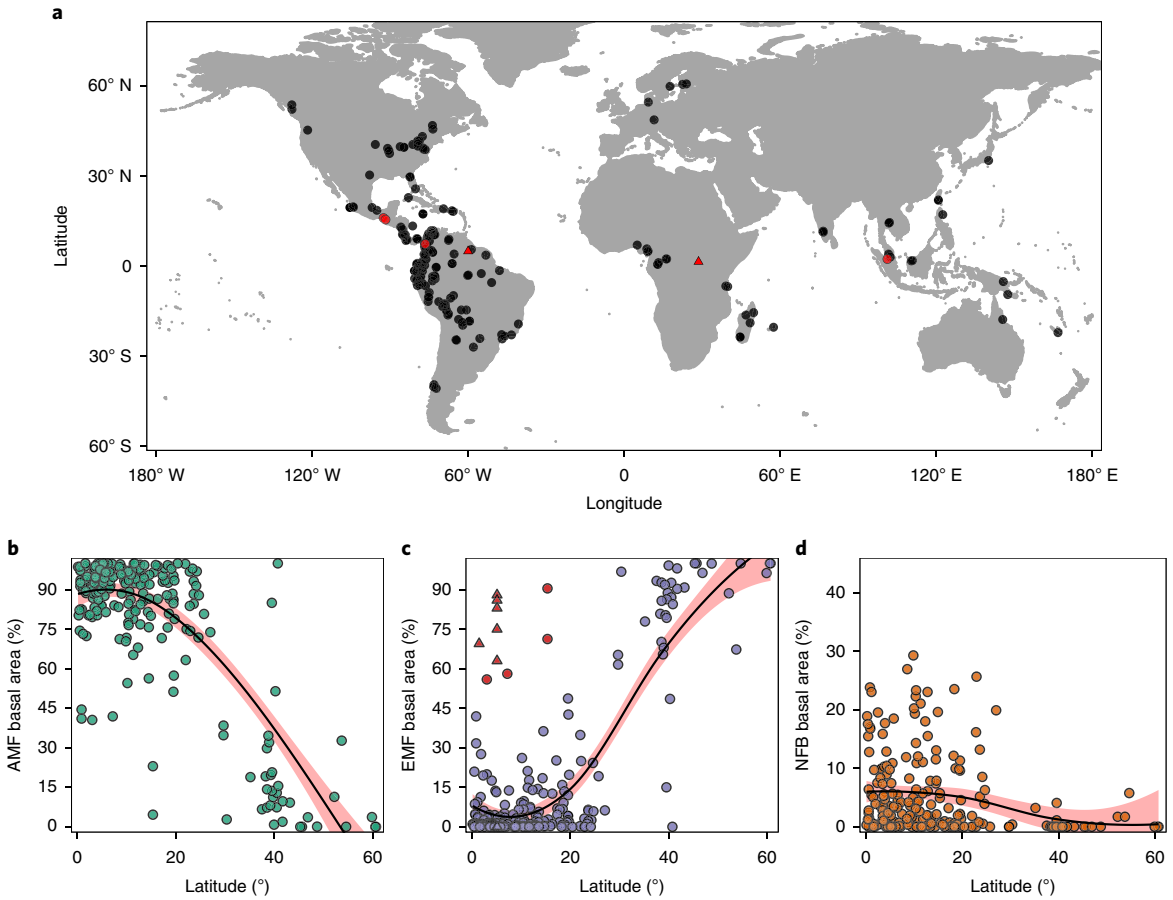

Fig. 2 | Global geographical distribution of AMF, EMF and NFB trees. a, Location of 225 Gentry vegetation plots (filled circles; 0.1 ha each) and 6 additional plots from the literature (filled triangles; 1–10 ha[72,73]). Red symbols in **a** and **c** indicate tropical forest plots dominated by EMF trees (basal area > 50%). **b**, The relative abundance of AMF trees (green circles) deceases with latitude. **c**, The relative abundance of EMF trees (purple circles) increases with latitude. **d**, The relative abundance of NFB trees (orange circles) decreases with latitude. Latitude values in **b**, **c** and **d** are given independent of north or south hemispheres. Lines are LOESS fit (span = 1), with 95% confidence intervals indicated by red shading. For each trend, beta regression analyses confirmed high statistical significance ($n = 225$; $P < 0.001$).

increased immediately following disturbance, but declined rapidly due to competition with EMF and/or AMF after ~40–60 years of forest succession. However, in tropical forests, facultative fixers peaked following disturbance, and the NFB strategy persisted indefinitely at high abundance (~10%) within the plant community due to: (1) the ability of individual NFB trees to downregulate fixation and thus reduce the cost of competing against AMF[5]; and (2) the frequent recurrence of patch-scale disturbances, in which NFB was the favoured strategy. These results closely recreate the patterns observed for fixer abundances, fixation rates and the downregulation of fixation across tropical forest succession[7].

Our model further allows us to evaluate the role of succession in generating the biome-scale patterns of nutrient limitation seen in Fig. 3c–f. We quantified the strength of limitation as the percentage increase in plant biomass in response to simulated nitrogen or phosphorus fertilization (Supplementary Fig. 2d–f; Methods). For all biomes, limitation was strongest immediately following disturbance when the supply of soil nutrients could not keep up with the demand created by rapid biomass accumulation. In the tropical biome, nitrogen limitation occurred immediately following disturbance, but quickly transitioned to phosphorus limitation as forests aged and fixers brought in new nitrogen to the ecosystem (Supplementary Fig. 2f). Also, this result is consistent with field observations of tropical forest succession[7,28].

The occurrence of phosphorus limitation strongly depended on whether nitrogen fixers were present in our simulated forests. In temperate forests, phosphorus limitation was most common in the phosphorus-poor non-glaciated soils, with fixer abundance explaining 71% of the variation in the strength of phosphorus limitation ($n = 188$; $P < 0.001$). In early succession, forest patches

Table 1 | Emergent biogeochemical properties from landscape simulation plus biome-specific model parameters

Variable (units)	Boreal	Temperate	Tropical
(a) Prescribed biome-specific variables			
Disturbance rate, d (yr^{-1})	1/100	1/70	1/50
Maximum GPP, G ($tC\,ha^{-1}\,yr^{-1}$)	10	16	30
Nitrogen mineralization rate, m_N (yr^{-1})	0.003	0.011	0.025
Nitrogen deposition, I_N ($kgN\,ha^{-1}\,yr^{-1}$)	5.0	5.0	5.0
(b) Emergent carbon and nitrogen pools			
Plant biomass carbon ($tC\,ha^{-1}$)	31 (47[a])	74 (61[a])	121 (164[a]; 138[b])
Soil organic carbon ($tC\,ha^{-1}$)	156 (185[c])	164 (148[c])	76 (100[c])
Soil organic nitrogen ($tN\,ha^{-1}$)	8.9 (10.5[c])	8.7 (8.0[c])	5.9 (7.9[c])
Percent fixer biomass (%)	<0.5 (0.9[d]; <2[e])	2.5 (1.9[d]; <2[e])	8.4 (5.8[d]; 10[e]; 11[f]; 6–14[g]; 6[h])
(c) Emergent carbon and nitrogen fluxes			
GPP ($tC\,ha^{-1}\,yr^{-1}$)	4.0 (6.0[i])	9.7 (9.5[i])	21.4 (23.3[i])
Internal nitrogen cycling ($kgN\,ha^{-1}\,yr^{-1}$)	36 (48[j])	88 (71–75[j])	153 (141[b])
Nitrogen fixed by trees ($kgN\,ha^{-1}\,yr^{-1}$)	0.11 (<0.1[k])	1.3 (1.1[k])	8.5 (2.2[h]; 5.3[k]; 10[l]; 1–14[m])
Total nitrogen loss ($kgN\,ha^{-1}\,yr^{-1}$)	5.2 (4.7[n])	7.1 (5.6[n])	9.2 (10–15[f])
Dissolved inorganic nitrogen ($kgN\,ha^{-1}\,yr^{-1}$)	0.4 (0.24[n])	1.3 (0.3[n])	3.0 (4–6[o])
Gaseous nitrogen loss ($kgN\,ha^{-1}\,yr^{-1}$)	0.3 (1–2[p])	1.0 (1–2[p])	2.3 (8–20[p]; 2–9[q]; 1.9[r])
Dissolved organic nitrogen ($kgN\,ha^{-1}\,yr^{-1}$)	4.6 (4.5[n])	5.1 (5.3[n])	4.5 (5–10[s])

Each temperate biome value is the simple mean of values from the glaciated and the non-glaciated temperate biome. Figures in parentheses identify empirical values from the literature (see below). Model runs without the belowground symbioses resulted in fundamentally different predictions of the land carbon and nitrogen cycles (see main text and Supplementary Table 3). [a]From Table 3 in ref. [55]. [b]From ref. [56]—a tropical forest carbon pool from 12 forests with complete above- and belowground biomass estimates (carbon = 0.48 × biomass). We also evaluated internal nitrogen fluxes from ref. [56] using the simple mean of 31 moist tropical forests worldwide. We used a factor of 1.3 to scale aboveground litterfall to the total (above- plus belowground) internal nitrogen flux. [c]From ref. [5], which used a global dataset to calculate soil carbon and nitrogen content to a depth of 1 m. The modelled soil organic carbon was derived from organic nitrogen using the biome-specific carbon-to-nitrogen ratio in ref. [5]. [d]From analysis of the Gentry database (Methods), based on the mean percentage basal area. [e]From Fig. 2 in ref. [57]. [f]From ref. [10]—the legume basal area from 16 50-ha tropical forest plots. [g]From Fig. 1g of ref. [58]. [h]From ref. [7]. [i]From Supplementary Table 5 of ref. [45] and the Methods. [j]From ref. [59]. We used annual net mineralization of 7 natural coniferous forest (~46° N) to approximate the boreal forest value and 30 temperate forests (~43° N) to derive the temperate forest value. [k]From ref. [60]—symbiotic nitrogen fixation calculated based on 1, 1 and 5% fixer cover in boreal, temperate and tropical forest, respectively. [l]From ref. [23]. [m]From ref. [61]—values for primary and secondary forests. [n]From ref. [62]. Inorganic nitrogen loss rates are low due to the unpolluted nature of these South American forests. [o]From ref. [63]. [p]From ref. [64]. Our model generated gaseous nitrogen loss similar to ref. [64] ($10.7\,KgN\,ha^{-1}\,yr^{-1}$) if we used the high nitrogen deposition implied at steady state in ref. [65] (a nitrogen deposition of $33.5\,KgN\,ha^{-1}\,yr^{-1}$). [q]From ref. [66]. [r]From ref. [67]. [s]From ref. [68].

with abundant fixers were most strongly phosphorus limited while patches with few or no fixers were nitrogen limited (Supplementary Fig. 2e). In tropical forests, fixers were abundant throughout succession (Supplementary Fig. 2c) and explained 65% of the variation in strength of phosphorus limitation ($n = 371$; $P < 0.001$). Forest patches could be nitrogen limited in early succession if nitrogen fixers were absent or if fixation was not rapid enough to meet the nitrogen demand of the rapidly accumulating biomass (Supplementary Fig. 2f). These results are broadly consistent with observations from both the tropical and temperate biome: fixation and biomass growth of fixers can be phosphorus limited in both biomes[29–31], and tropical forests can switch from nitrogen limitation in early succession to phosphorus limitation in later stages[7,28,32]. We conclude that feedbacks between belowground symbiotic strategies, forest disturbance and succession are critical for determining the emergence of biogeochemical cycles at the biome scale.

AMF–EMF bistability: theoretical and empirical evidence. Soil fertility affected the abundance of each strategy in each biome (Supplementary Fig. 3 and Supplementary Note 6). For example, both EMF and NFB deceased with deceased cycling of plant-available phosphorus, as AMF gained a comparative advantage due to enhanced phosphorus limitation.

In the tropical biome, our model predicts the existence of AMF–EMF bistability in conditions of low-fertility soils combined with low disturbance (Fig. 4a), as observed empirically[21,33]. Either strategy could dominate a local patch, but neither could invade the other once plant–soil feedback was established (Supplementary Fig. 4 and Supplementary Note 7).

Bifurcation analysis further showed that there exist conditions under which the initial tree establishment determines the divergence of the two alternative stable states under the same initial soil condition (Fig. 4b). This biogeochemical founder effect offers a mechanism to explain how two alternative plant–soil–nutrient economies[13,34] can emerge in nutrient-poor tropical soils (Fig. 2c; red versus purple points) and in temperate landscapes (discussed below): one based on organic (EMF) and one on inorganic nutrient cycling (AMF). Our model thus identifies intrinsic biological feedback—between plant symbiotic strategies and their collective effect on the plant–soil–nutrient cycle—that can generate community composition independent of conditions external to the biological system (for example, soil, climate and so on).

Next, we tested our model's ability to resolve plot-level distributions of plant symbiotic strategies across the biomes in Gentry's global dataset ($n = 225$ plots). We assumed that: maximum GPP (G) differed across biomes (Table 1); nutrient mineralization (m) and ecosystem disturbance (d) declined with increasing latitude (due to the effect of temperature on both processes); and soil phosphorus was higher in glaciated regions (Table 1; Methods). In addition, to mimic the influence of disturbance on AMF versus EMF distributions in real-world plots, we allowed our predictions to be influenced by disturbance as a stochastic factor (Methods).

Across the Gentry dataset, our model could account for the majority of plot-level variation in community composition, explaining 68% of variance in EMF and 65% of variance in AMF abundance (Methods). Between-plot NFB predictions are inherently more difficult (5% explained) as nitrogen fixation in nature depends on disturbance history and is therefore subject to stochastic variation.

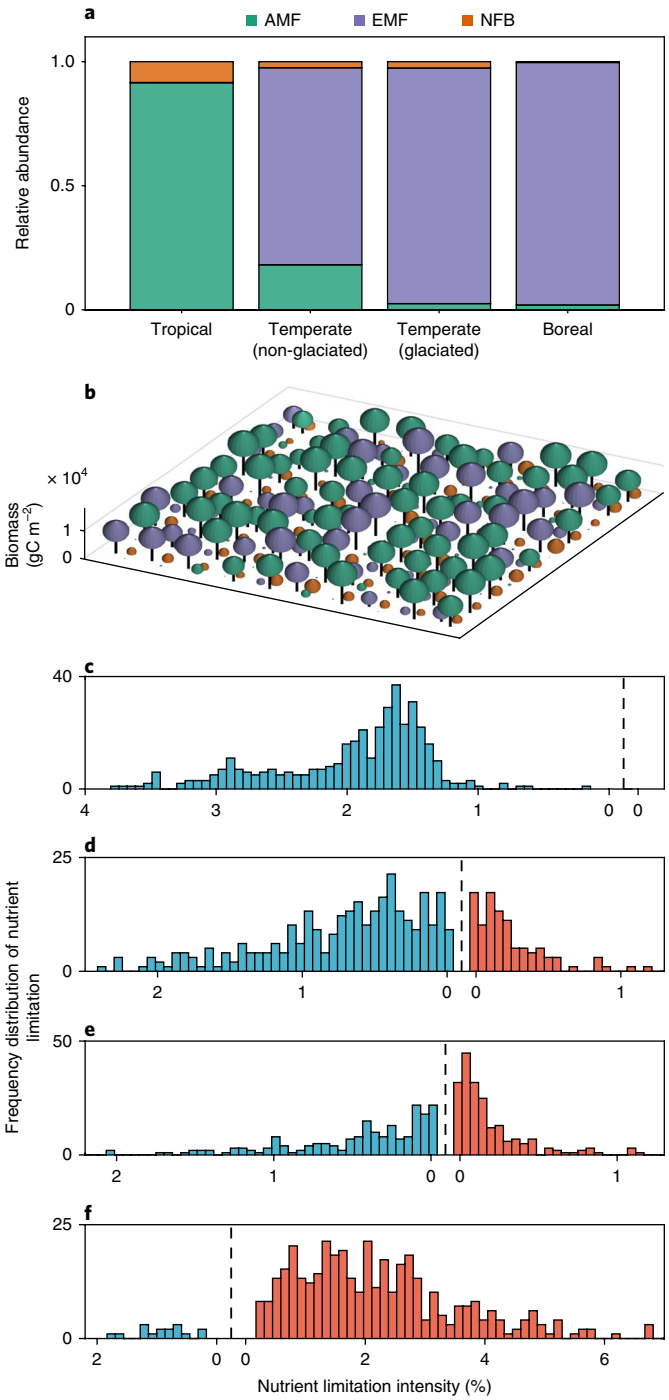

Fig. 3 | Prediction of community composition and nutrient limitation across biomes. a, AMF (green), EMF (purple) and NFB (orange) symbiotic strategies across biomes. Values are averages of 400 forest patches simulated over 10,000 years and subject to biome-specific conditions of external disturbance (*d*), nutrient mineralization (*m*), weathering input of soil phosphorus (l_p) and maximum GPP (*G*). The NFB emergent ESS is facultative in tropical but obligate in temperate and boreal biomes (Supplementary Fig. 1). **b**, Schematic of a simulated landscape of low-fertility tropical forest consisting of 100 individual patches. Tree height and crown size are proportional to patch biomass, while the tree crown colour indicates the symbiotic strategy. **c**–**f**, Frequency distribution of the quantitative strength of nutrient limitation in boreal (**c**), glaciated temperate (**d**), non-glaciated temperate (**e**) and tropical forests (**f**). Nitrogen limitation is shown in blue and phosphorus limitation in red. The biome results show a shift in nutrient limitation from predominant nitrogen limitation in boreal and glaciated temperate forests to an increased frequency of phosphorus limitation in non-glaciated temperate forests, and predominant phosphorus limitation in tropical forests. We performed *in silico* fertilization experiments on a landscape of 400 forest patches by applying, over 10 years, either nitrogen or phosphorus at levels that were 10 times the background input (Methods). For each patch, the strength of nutrient limitation was calculated as the percentage difference in plant biomass between the fertilized and unfertilized landscapes.

Our model was generally accurate in boreal and tropical forests, with >93 and >81% of the respective plots predicted within an absolute discrepancy of 10% for either the EMF or AMF strategy. However, a small fraction (7%) of plots in tropical forests and a larger fraction (46%) in temperate forests differed more than 25% from our predictions. Such large divergence in the distribution of AMF versus EMF abundances may arise from the bistable competitive dynamics discussed above, where initial conditions determine which strategy will dominate in a given plot.

Next, we evaluated the potential emergence of bistability within the temperate biome, by analysing tree community composition across 212,182 plots of naturally regenerated forest in the Forest Inventory and Analysis (FIA) database of the US Forest Service. First, we calculated the observed symbiotic composition across all plots and evaluated the distribution of symbioses across latitude, from Puerto Rican tropical forests to Alaskan boreal forests. In Fig. 5a, we show the distribution of EMF relative abundance across latitude, based on a random subset of 6,159 plots stratified by latitude (Methods). The analogous plots for AMF and NFB are shown in Supplementary Figs. 5 and 6.

The observed plot-level composition confirms the observed (Fig. 2) pattern of: (1) low EMF and high AMF abundance in low-latitude tropical forests (<25° N); (2) high EMF and low AMF abundance in high-latitude temperate and boreal forests (>40° N); and (3) AMF and EMF coexistence in intermediate temperate latitudes (25–40° N). Frequency distributions of both EMF and AMF abundances (Fig. 5b–e and Supplementary Fig. 5, respectively) show that both high and low latitudes are characterized by unimodal distributions, while the temperate biome displayed a more complex pattern. Notably, forests between ~25–35° N latitude (red points in Fig. 5a; Methods) are dominated by either the EMF or AMF strategy, consistent with expectations for a bistable pattern as discussed above (Fig. 4a).

As for the Gentry dataset analysis, we used plot-level predictions to evaluate the distribution of EMF versus AMF strategies in FIA plots across latitude (Methods). Our results closely recreate the observed latitudinal pattern in Fig. 5a, including the unimodal EMF and AMF abundances in high- versus low-latitude forests, respectively, and the bimodal distribution in the 25–35° N latitude region of temperate forests.

The emergence of a bimodal distribution is consistent with bistable dynamics in the competitive relationship between EMF and AMF strategies, as indicated empirically in local-scale experiments[4]. The pattern is also consistent with the theoretical prediction[35] that ecosystems can display co-occurring alternative stable states—or 'flickering'—as they transition from one state to another—from AMF to EMF dominance, in our case. These results imply that plant–soil feedbacks that are mediated by specific symbiotic relationships can scale up to stochastic patterns that emerge at scales within and between biomes.

Emergence of global biogeochemical cycles. Finally, we evaluated our model's ability to predict the emergence of carbon, nitrogen and phosphorus cycles at global scales. In Table 1, we compare

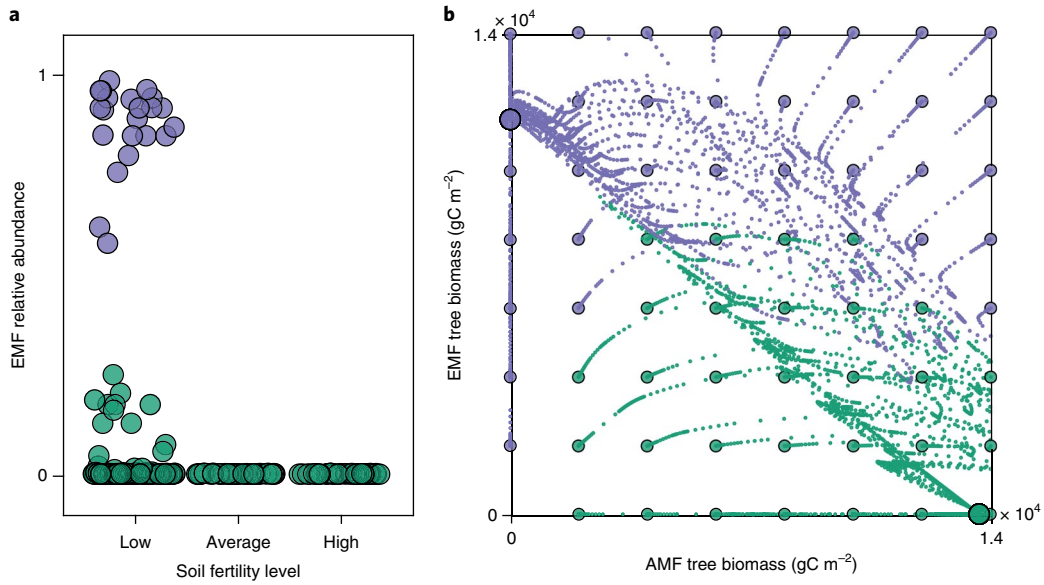

Fig. 4 | AMF–EMF bistable states in low-fertility tropical forest, and divergence of communities into alternative stable states. a, Relative abundance of EMF trees in low-disturbance tropical forests across a gradient of soil fertility. Purple circles indicate forest patches where EMF dominates (>50% of biomass) and green circles represent patches where AMF dominates. AMF is the dominant strategy in conditions of medium and high soil nutrient mineralization, but EMF and AMF are alternative stable states in conditions of low mineralization. **b**, Forest patches that start from different combinations of initial AMF and EMF abundances (small circles) will, over time, produce two alternative equilibrium communities: one dominated by AMF (large green circle) and one by EMF (large purple circle). This founder effect shows that internal biotic interactions can determine the fate of competition between trees that employ different belowground strategies. We performed this analysis using a constant, rather than stochastic, disturbance rate, which is required to demonstrate the trajectory of individual trends (dotted lines).

biome-specific predictions with consensus literature observations of plant and soil biomass distributions, forest productivity, and nitrogen fixation, cycling and loss (see Supplementary Table 2 for an analogous phosphorus table). Despite its simplicity, our model closely predicts global-scale variations in these nutrient cycles, including patterns of nitrogen fixation, carbon and nutrient cycling, and observed patterns and rates of nitrate leaching and denitrification.

Moreover, our findings indicate that belowground symbioses are critical for these global cycles (Supplementary Table 3). For example, the rates of net primary production and forest internal nitrogen and phosphorus cycling dropped by ~48% in tropical forests and ~19% in boreal forests when we modelled a world without symbioses. The drop in forest biomass was roughly equivalent to these declines, but biome-specific gross primary production (GPP) declined less (21% in tropical forests and 11% in boreal forests), indicating that the evolutionary emergence of belowground symbioses has caused net primary production to become more efficient (that is, a higher net primary production-to-GPP ratio) in the land biosphere.

Conclusions

The relationship between natural selection, symbiosis and nutrient cycles is an open area for scientific advancement. Perhaps the most compelling aspect of our results is the indication that a low-dimensional (limited number of governing equations and assumptions) first-principle model framework can merge these disparate areas and, in doing so, predicts the emergence of broad patterns in plant diversity, nutrient cycling and ecosystem bistability.

Specifically, the biome-scale impact of symbiotic nutrient strategies can be understood from: (1) the influence of biome-scale drivers on nutrient demand and supply (G, m, d and I_P); (2) the cost–benefit trade-off associated with each strategy; and (3) the ability of specific plant strategies to interfere with local plant–soil–nutrient cycles: by reducing mineralization and short-cutting the uptake of plant-available nutrients (EMF symbiosis) or adding new nitrogen to plants and soil (NFB symbiosis). The resulting predictions can resolve distributions of belowground plant strategies, the sequence and timing of forest succession, the emergence of AMF–EMF bistability and broad properties of carbon and nutrient cycles in the land biosphere.

We conclude that, as a consequence of land plant evolution, belowground symbioses have been a key force influencing plant communities, and that, in turn, the resulting plant–soil–nutrient feedbacks have shaped global carbon and nutrient cycles. A better mechanistic representation of these feedbacks in global models may reduce uncertainties in our projections of future vegetation dynamics and biogeochemical cycles.

Methods

Global distribution of plant belowground nutrient strategies. We compiled a global dataset to investigate the geographical pattern of belowground symbiotic strategies across forest biomes. We analysed Gentry's[36] quantitative vegetation survey of 225 sites distributed worldwide across tropical, temperate and boreal forests and undisturbed by human activities ('pristine'; *sensu* ref. [36]). At each site, we calculated the percentage basal area for each tree species (lianas excluded) present by summing across individual trees. We considered all of Gentry's study locations (Fig. 2) and, in each location, all observations of trees with a diameter of >2.5 cm at breast height.

We classified each species as belonging to one of four strategies: fixer (symbiotic nitrogen-fixing bacteria housed in root nodules; NFB), miner (symbiotic ecto- and ericoid mycorrhizae; EMF), naked root (no symbiotic association) and scavenger (symbiotic arbuscular mycorrhizae; AMF). We combined ecto- and ericoid mycorrhizae into a single functional group, but individual species vary in their mining ability, with ericoid mycorrhizae (common in high-latitude ecosystems) generally thought of as most capable[18,37,38].

Our classification was based on authoritative databases in the literature, and our own compilation of data as follows. First, we determined whether a tree species is capable of symbiotic nitrogen fixation using Janet Sprent's global legume database[14] (4,126 rhizobial species across 366 genera in the 3 subfamilies that make up the legume family). For non-legume fixer species, we used 4 review papers[39–42], which together identified 201 actinorhizal plant species across 26 genera. We used genus-level information for any species absent in these databases, as, with few exceptions, fixation is a conservative trait at the genus level (J. Sprent,

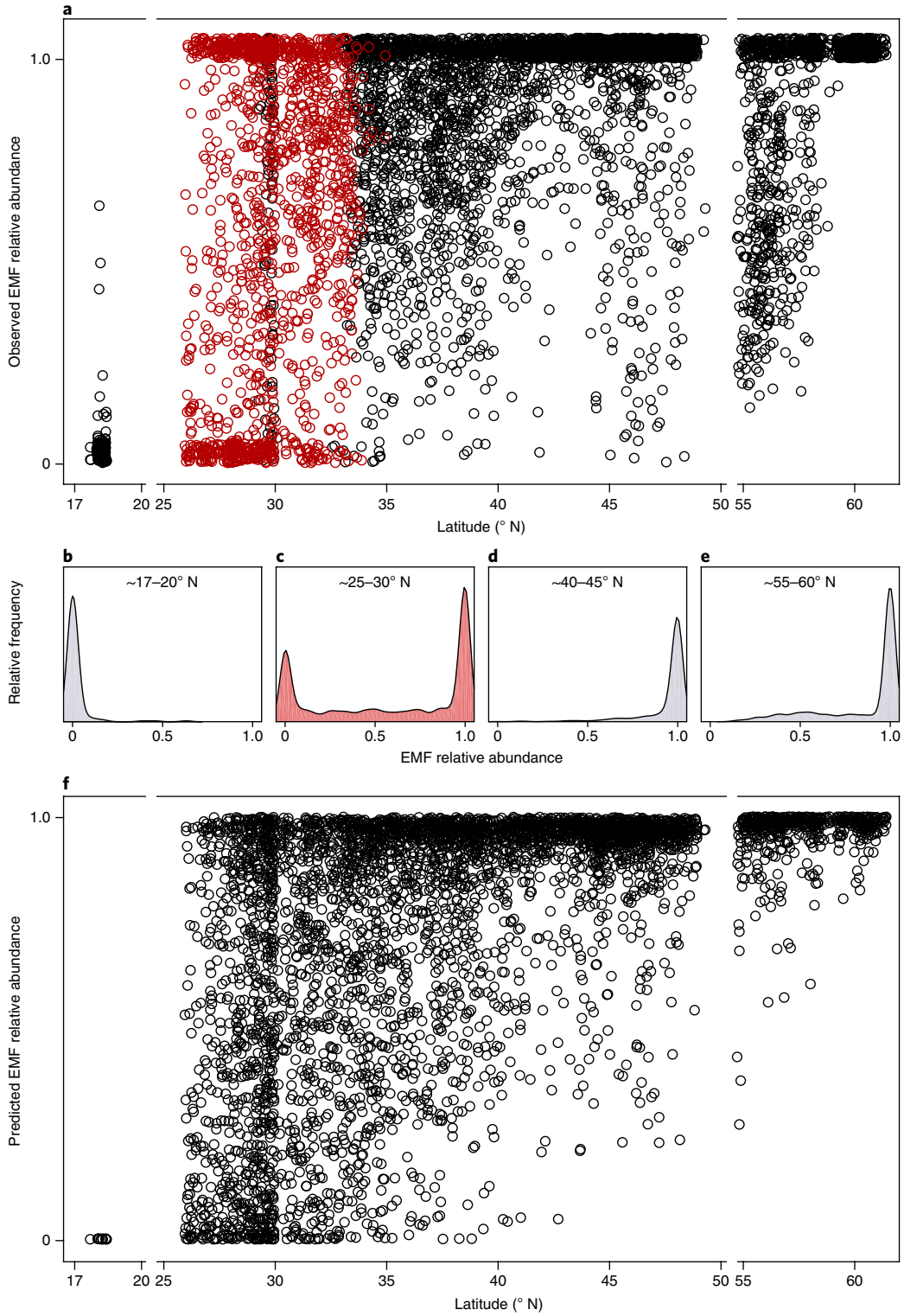

Fig. 5 | Observed and predicted EMF relative abundances across the US FIA plots, and bistable dynamics in the temperate region. a, Observed EMF tree basal area of each FIA plot ($n = 6{,}159$) across latitudes from southern Puerto Rico (17.8° N) to Alaska (61.5° N). AMF dominates over EMF in southern plots (<25° N), but EMF increases with latitude and becomes dominant in northern plots (>35° N). Red circles identify the region of AMF–EMF bistability derived from our statistical procedure (Methods). A 5% random jitter was added to the *y* axis for better visibility of overlapping points. **b**–**e**, Frequency distribution of the relative EMF abundance across four latitudinal bands. EMF is rare in the low-latitude tropical island of Puerto Rico (**b**), but shows unimodal dominance in the high-latitude Alaskan boreal forest (**e**). Across temperate North America, EMF shifts from bimodal coexistence with AMF (that is, bistable conditions; **c**) to unimodal EMF dominance as latitude increases (**d**). The area under each frequency curve equals 1, and the curve in **c** is red to note the link to the red points in **a**. **f**, Model prediction of EMF relative abundance for each FIA plot in **a** ($n = 6{,}159$). The conditions for this stochastic model run are given in the Methods.

personal communication). Second, we determined whether a species employs ecto- or ericoid mycorrhizae (that is, the miner strategy) using a database that we compiled as follows. We used Wang and Qiu's 2006 global dataset[43] on belowground mycorrhizae associations of 3,033 species across 1,408 genera. We further expanded this dataset by searching (search terms = 'ectomycorrhizal' or 'ectomycorrhizae' and 'tree' and publication year later than 2006) for more recent publications that identify new ecto- and ericoid mycorrhizal relationships ($n = 73$ species across 22 genera). Third, for the naked root strategy, we used species identified as exclusively non-mycorrhizal in the Wang and Qiu dataset. We found <0.01% naked root species across Gentry's plots, consistent with the idea that non-mycorrhizal trees are rare in nature and predominately occur in conditions where forest cannot establish (for example, aquatic habitats, parasitic or carnivorous strategies)[17,44]. Finally, we classified tree species that were not employing fixer, miner or naked root strategies as arbuscular mycorrhizae species (that is, the scavenger strategy).

While the goal of each dataset[14,39–43] has been to characterize belowground strategies across land plant taxa, it is difficult to evaluate whether they represent the full taxonomic spectrum that exists across regions worldwide. Each dataset was built from individual studies that typically focused on local scales, but each dataset is composed of observations from locations and biomes that range broadly. To the extent that symbiotic relationships are constrained taxonomically[14,43], our approach allows us to use local measures of tree community composition to infer patterns of belowground nutrient strategies across broad geographic regions.

Model description. Our model evaluates the adaptive dynamics of individual trees that interact within a local plant–nutrient cycle and that deploy different strategies for belowground symbiotic nutrient acquisition. The approach expands on a previous analysis[5] limited to NFB, but we now incorporate a global ensemble of belowground strategies and explicitly model the emergence of local plant–soil–nutrient feedbacks. Each strategy imposes a different cost on the tree carbon economy, and thereby on tree fitness, as outlined below. In contrast with traditional optimization models, our ESS approach allows for incremental mutation in plant strategies and traits, and lets mutant and resident trees compete across strategy and trait space. The resulting ESS may or may not coincide with the results of traditional ecosystem optimization analyses. Model predictions were generally robust to differing assumptions about cost trade-offs and prescribed variables (Supplementary Notes 2–6).

Our model employs three fundamental equations—equations (1)–(3), discussed below: equation (1) in Box 1 describes the growth of tree biomass (B) as a function of the intrinsic growth rate (g), biomass turnover caused by the intrinsic mortality of trees and/or tree tissues (μ) and tree turnover caused by externally imposed disturbances (d), such as wind-throw, landslides, fire, and so on. Following meta-analyses across biomes[26] (Table 1 and Supplementary Note 5), we allowed disturbance-related turnover (d) to range from high (~1/50 yr^{-1}) in tropical, to medium (~1/70 yr^{-1}) in temperate, and low (~1/100 yr^{-1}) in boreal forests.

Equation (1a) in Box 1 shows that—in carbon-limited conditions—the plant intrinsic growth rate (g_C) depends on the balance between carbon income from gross photosynthesis and carbon loss. Carbon loss, in turn, consists of plant tissue respiration (δ; carbon respired per biomass) plus the cost of employing different belowground strategies where θ quantifies the nutrient–carbon trade-off (carbon expended per soil nutrient acquired) at the maximum rate of nutrient uptake: scavenging = θ_S, mining = θ_M, fixation = θ_F and naked root uptake = θ_v. In addition, facultative nitrogen-fixing plants pay an opportunistic cost (ψ) for maintaining the facultative strategy[5].

Equation (1b) in Box 1 describes that—in nutrient-limited conditions—the tree growth rate (g_i, where the subscript i denotes either nitrogen or phosphorus) depends on the assimilation rate of the nutrients, which, in turn, is governed by the carbon investment into each specific uptake strategy: (1) scavenging of nitrate, ammonium, phosphate or amino acids from the plant-available soil nutrient pool (A_i) at the rate S_i and the half-saturation constant c_i^S (that is, AMF symbiosis); (2) mining of organic nutrients from the soil organic-bound nutrient pool (O_i) at the rate M_i and the half-saturation constant c_i^M (that is, EMF symbiosis); (3) fixation of atmospheric di-nitrogen at the rate F_N using an either obligate or facultative fixation strategy[5] (that is, NFB symbiosis); and (4) naked root uptake of plant-available soil nutrient at the rate v_i and the half-saturation constant c_i^v (that is, no symbiosis).

In each biome (j), gross photosynthesis increases with aboveground biomass (αB, where α is the aboveground fraction of total plant biomass, B), is characterized by the half-saturation constant c_G and saturates at maximum GPP (G_j). For simplicity, we conservatively estimated G_j as 1.2 times the highest biome-specific GPP reported in ref. [45], ranging from high (~30 t C ha^{-1} yr^{-1}) in tropical, to medium (~16 t C ha^{-1} yr^{-1}) in temperate, and low (~10 t C ha^{-1} yr^{-1}) in boreal forests (Table 1).

Individual tree dynamics are modelled within a locally resolved nutrient cycle that tracks two soil pools: organic-bound (O_i; equation (2)) and available (A_i; equation (3)) nitrogen or phosphorus.

$$\frac{dO_i}{dt} = (\mu_X + d_j - \tau_i d_j)\frac{B}{\omega_i} - \left(m_j(1+\sigma_X) + \phi + \frac{M_i(1-\alpha)B}{O_i + c_i^M}\right)O_i \quad (2)$$

Equation (2) describes how O_i depends on four terms: (1) input from tree biomass turnover (μ); (2) loss to nutrient mineralization (m); (3) loss to hydrological export (ϕ); and (4) loss to plant symbiotic mining (M_i). Tree biomass turnover is caused by tree mortality and tissue turnover (μ) plus external disturbance (d), with a correction term (τd) in which τ defines the proportion of each nutrient lost by hydrological or gaseous export following a disturbance event. To capture the greater propensity for nitrogen to be lost and phosphorus to be recycled following disturbance, we assumed that $\tau_N = 0.1$ and $\tau_P = 0$, and that d differs across biomes as described above. Finally, based on field studies, we considered that nitrogen fixers turn over (μ_F) ~20% faster than non-fixers (Supplementary Note 4).

The nutrient mineralization rate constant (m_j) increases with mean annual temperature across biomes[46] (Table 1). In addition, our model considers the well-known inhibitory effect of the EMF symbiosis on soil nitrogen mineralization (Supplementary Note 4) using a term (σ_X) that modifies the biome-specific m_j, and where $\sigma_M = -0.36$ and $\sigma_S = \sigma_F = 0$ based on a recent global analysis[47]. Mechanistically, this inhibition effect can be attributed to the litter of EMF plants (for example, a high carbon-to-nitrogen ratio and high lignin content) and/or the fungal partner employed (for example, the ability to compete against saprotrophic microbes for nutrients or water), as described in Supplementary Note 4.

Hydrological loss (ϕ) occurs in the form of dissolved organic-bound nutrient compounds that leach out of the soil pool and exit the ecosystem. Finally, plant symbiotic mining (M) transfers nitrogen or phosphorus from the organic-bound pool to plant biomass as described above:

$$\frac{dA_i}{dt} = I_i + m_j(1+\sigma_X)O_i - \left(k + \frac{S_i(1-\alpha)B}{A_i + c_i^S} + \frac{v_i(X)(1-\alpha)B}{A_i + c_i^v}\right)A_i \quad (3)$$

Equation (3) defines the change in plant-available nutrient (A_i) in response to four terms: (1) input from atmospheric deposition and/or geological weathering (I_i); (2) input from organic matter mineralization (m); (3) loss to hydrological export (k); and (4) loss to plants via scavenging (S_i) and naked root uptake (v_i). The mineralization rate constant (m) is modified by the term σ_X, as discussed for equation (2) above. The uptake of plant-available nutrients depends on the scavenging (S_i) or naked root uptake (v_i) rates, as described in equation (1b) above.

Estimation of cost coefficients. We calculated the carbon cost for the different belowground strategies as follows (see Supplementary Note 1 for a complete description). We express miner and scavenger carbon costs per unit nitrogen, but note that this value can be converted to a per-unit phosphorus cost by multiplying it with the stoichiometric phosphorus versus nitrogen uptake ratio (Box 1). For NFB, we estimated the metabolic cost of the fixation process from published studies and values used in previous models: $\theta_F = 10$ gC/gN acquired by fixation. Following ref. [5], we also included the opportunistic cost of maintaining a root structure capable of both fixation and competition for soil nutrients by facultative nitrogen fixers: $\psi = 25$ gC/gN. For EMF, we evaluated studies of the carbon balance of forest stands with EMF trees combined with field estimates of the percentage of plant nitrogen derived from the EMF symbiosis: $\theta_M = 5$ gC/gN. To derive the AMF cost from published studies, we considered that AMF plants generally invest less carbon into hyphae (compared with the extensive EMF hyphae network), rely less on the excretion of carbon-rich molecules or extracellular enzymes and derive a smaller fraction of total nitrogen from the symbiosis. Based on published data, we estimate $\theta_S = 2$ gC/gN. For naked roots, we bear in mind that the carbon cost of active nitrogen uptake through absorptive root surfaces is small compared with the NFB, EMF or AMF symbioses. We used the value $\theta_v = 0.5$ gC/gN. We performed sensitivity analyses to assess the uncertainty of this overall cost structure, as detailed in Supplementary Note 2.

Representation of plant symbiotic strategies and Darwinian trait evolution. We consider that plants possess whole-plant strategies (scavenger, miner, fixer and naked root) that have evolved to benefit the plant's ability to acquire nutrients in competition with neighbouring trees, but that are also influenced by fundamental cost trade-offs. To create a trait-based model subject to Darwinian evolution, we identify each belowground strategy with a single quantitative trait, X, that governs the rate of nutrient uptake at a given carbon cost: inorganic scavenging (S), organic mining (M) and symbiotic fixation (F). For each trait, we consider a spectrum of mutants that range from 'no symbiosis' (that is, $X = 0$) to maximum symbiotic investment (that is, $X = \overline{X}$). This range is consistent with observed gradients of investment in AMF, EMF or NFB symbioses across different tree species.

In the case of the fixer strategy, observations in natural forests have shown that some tropical and subtropical trees can downregulate their fixation rate in conditions of abundant soil nitrogen (where carbon-costly fixation is not competitively favoured) or growth under a closed canopy (where light is insufficient to fuel fixation). We therefore distinguish a facultative fixation strategy[5,7,10,24,48] in which fixers can instantaneously adjust their fixation rate (F_j; Supplementary Fig. 1) to balance carbon and nutrient uptake at the whole-plant level. As a result, plants that grow in high-nitrogen soils will downregulate fixation in response to abundant root nitrogen uptake, while plants under low-light conditions will reduce fixation in response to reduced biomass growth and nitrogen demand. We further define trees that lack the capacity to downregulate fixation[5,25,49] as obligate fixers, as these fixers display a constant fixation rate independent of local soil and light conditions. Finally, we allowed

each fixer strategy to be associated with either AMF or EMF mycorrhizal fungi (Supplementary Table 1), as observed in nature.

Fundamental biological trade-offs. From a biogeochemical perspective, the seemingly diverse strategies by which plants forage for belowground nutrients share two fundamental trade-offs. By employing symbionts, a plant can access nutrient sources (soil inorganic, soil organic or atmospheric pools) that naked roots cannot exploit, or at concentrations that are lower than those naked roots can consume (that is, lower half-saturation constants for uptake). However, this action carries two trade-off costs: (1) the plant sacrifices photosynthetically acquired carbon that could otherwise be used for above- or belowground biomass growth (that is, nutrient–carbon trade-off; equation (1a) above and Supplementary Note 1); and (2) the plant sacrifices the ability to acquire nutrients through the lower-cost naked root, as symbionts housed within the rooting system (for example, the EMF hyphae sheath that encapsulates rootlets) physically interfere with the per-biomass root absorptive surface area available for direct nutrient uptake (that is, uptake trade-off; Supplementary Note 3).

We represent the resulting trade-off in equation (4), with root nutrient uptake decreasing with increased symbiont colonization. In the absence of physiological measures, we assumed that this trade-off is linear, following ref. [5]. $\bar{v}$ is the uptake capacity of a naked root in the absence of symbiont colonization (that is, the maximum naked root uptake rate) and v'_X is the maximum reduction of the root uptake rate at the maximum symbiotic uptake rate $\overline{X}$. In turn, the ratio $X/\overline{X}$ quantifies the load of symbionts relative to the maximum potential for each strategy. The physiological upper limit of $\overline{X}$ was approximated from empirically observed fixation or plant uptake rates in natural forests (for example, refs. [5,11]):

$$v(X) = \bar{v} - v'_X \frac{X}{\overline{X}} \quad (4)$$

ESS analysis. We simulated natural selection and evolution by allowing random trait mutants to arise within resident plant populations, within the context of plant–soil nitrogen and phosphorus cycles in equilibrium with the resident population. We examined the outcome of competition between all paired combinations between a resident (that is, a specific trait value, X) and any mutant strategy. We numerically determined whether a 1% mutant introduction (by biomass) at equilibrium could invade and/or replace the resident[5], given the biogeochemical and light conditions that are set by the resident (Supplementary Note 10). The ESS is the resident X that cannot be eliminated by any other strategy within the plant–soil nutrient cycles created by the resident.

We conducted the ESS analysis across all mutants and strategies. The resulting community-level ESS (indicated by the red star in Supplementary Fig. 1) is the resident strategy that cannot be eliminated by any mutant across all possible strategies. We examined the undisturbed forest community-level ESSs by setting external disturbance (d) to zero. We then considered disturbed forest community-level ESSs by setting d to 1/20 yr^{-1} (that is, 20-year-old forest, on average) and by allowing higher nitrogen loss ($\phi = 0.0075\ yr^{-1}$). These conditions create an early succession quasiequilibrium, which is required since ESS can only be evaluated at equilibrium.

Modelling biome-specific differences. We kept all external and internal variables (Supplementary Table 1) the same across biomes, except for allowing: (1) the maximum GPP (G) to increase with decreasing latitude; (2) the external phosphorus input (I_P) to be elevated in glaciated regions; (3) the mineralization rate constant (m) to increase with decreasing latitude; and (4) the external disturbance rate (d) to increase with decreasing latitude (Table 1). Properties at the ecosystem scale (that is, forest community composition, successional trends, bistability, and carbon, nitrogen and phosphorus cycles) therefore emerged as a consequence of the interaction of these four assumptions with plant strategies within forests.

Landscape dynamics analysis. Natural forests consist of vegetation patches that differ in age since disturbance, forming a successional landscape mosaic that is not adequately represented by traditional homogenous models. To evaluate competitive dynamics and nutrient cycles in such mosaic forests, we seeded a landscape of 400 patches with the community-level ESS strategies (for strategies with no community-level ESS, we included the best-performing mutant) derived in the analysis above (Supplementary Fig. 1). We evaluated differences across boreal, glaciated temperate, non-glaciated temperate and tropical forests by varying G, I_P, m and d as described above and in Table 1. All other factors and variables were kept the same as noted above. The forest patches were subject to stochastic disturbance at the biome-specific probability d_j. Each disturbance event killed two-thirds of living biomass, with a fraction τ_N (10%) nitrogen in killed biomass lost to hydrological and/or gaseous export, and the remaining fraction (90%) recycled within the ecosystem (sensitivity analysis detailed in Supplementary Note 5).

Since m differs between EMF and other strategies, we separately tracked soil organic nitrogen and phosphorus generated by each strategy; we applied a strategy-specific mineralization rate ($m_X = m_j \times (1 + \sigma_X)$) in each forest patch.

The landscape dynamics is visually demonstrated in Supplementary Video 1.

Biome-level nutrient limitation. We evaluated the form and extent of nutrient limitation at the individual patch level. In each biome, we seeded a landscape of 400 patches with community-level ESS AMF, EMF and NFB plants and let it run for 10,000 years in the conditions detailed above. We then duplicated this landscape in conditions of ten times the external input of either nitrogen or phosphorus, to mimic a nutrient fertilization experiment. In addition to evaluating whether nitrogen or phosphorus limited plant growth, we calculated the strength of limitation in each patch as the percentage difference in plant biomass between the fertilized versus unfertilized landscape. To examine the association between limitation and either disturbance or plant community composition, we: (1) calculated the time since the most recent disturbance for each fertilized plot; and (2) quantified the composition of AMF, EMF and NFB at the time of initial fertilizer addition in each plot.

Succession dynamics analysis. We evaluated secondary succession in a 400-patch landscape by introducing a disturbance event that reduced all patches to a fraction (5% in the Supplementary Fig. 2a–c) of their original biomass. Nutrients in the killed biomass were transferred to the soil organic nutrient pool and hydrological/gaseous losses, as discussed above. Each forest patch regenerated from a collection of seeds drawn from the community-level ESS strategies for each given biome. We seeded a consistent percentage (30%) of NFB across all biomes, to allow for direct comparison across biomes and to ensure that the resulting trends were not subject to the stochastic influence of small seed numbers. To account for observed trends in dominant strategies across biomes, we held non-fixers as exclusively EMF in boreal forests, exclusively AMF in tropical forests, and half AMF and half EMF in temperate forests. We tracked community composition, and carbon and nutrient accumulation in vegetation and soils, over ecological time (400 years).

The FIA dataset. We analysed the FIA database of the US Forest Service, which contains information on forest community composition across 1 ha plots across the United States, including Puerto Rico and Alaska. With the assistance of J. Lichstein at the University of Florida, we selected 534,106 plots that were sampled by in-person ground surveys. We then further refined this dataset to select: (1) naturally regenerating forest plots; (2) 100% of the plot areas sampled; and (3) plots for which we could confirm accurate GPS coordinates. For each of the resulting 212,182 plots, we calculated the percentage basal area for each tree species present by summing all living trees with a diameter >2.5 cm at breast height. We then classified species according to their symbiotic strategies using the same method used for our Gentry dataset analysis. For clearer visual and statistical interpretation in Fig. 5, we selected a subset of 6,159 plots as follows: we stratified plots into 7 latitudinal bands (<25, 25–30, 30–35, 35–40, 40–45, 45–50 and >50° N latitude) and randomly sampled 1,000 plots from each band. Only 159 plots were available in the <25° N latitude band of Puerto Rico.

Plot-level abiotic factors. We acquired the following abiotic conditions for each Gentry and FIA plot: (1) elevation; (2) mean annual temperature; (3) annual temperature range; (4) annual precipitation; (5) precipitation seasonality; (6) harmonized soil quality; (7) soil texture; and (8) glaciation status. We derived elevation from the Google Elevation API (elevation function, R package 'rgbif'). Each climatic variable was derived from the 30-year (1970–2000) average at 1 km spatial resolution from WorldClim Version 2 (ref. [50]) (http://worldclim.org/version2). Soil quality data are from the crop production map of the Harmonized World Soil Database version 1.2 (ref. [51]); we averaged the measures of nutrient availability and nutrient retention into a single soil-quality index; both measures are strongly correlated. We acquired soil texture, including the percentage of sand and percentage of clay content, from Soil Grids (https://soilgrids.org). Lastly, we determined the glaciation status of each plot by evaluating whether or not each plot falls within the extent of the ice sheets during the Last Glacial Maximum (digitalized from a glaciation map of *Encyclopædia Britannica* (2014)).

Detection of bistability in the FIA dataset. We developed a statistical approach to detect the presence of AMF–EMF bistability in a given population of FIA plots. Specifically, we evaluated whether an observed bimodal distribution pattern (for example, Fig. 5c) could emerge due to natural heterogeneity in underlying environmental factors including soils and/or climate. For example, the coexistence of rich versus poor soils could generate a bimodal distribution of AMF and EMF in any latitudinal region of Fig. 5. If the underlying abiotic factors could not explain the observed bimodal distribution, we inferred that the distribution was probably generated by a bistable community assembly process (shown as red points in Fig. 5).

Specifically, we chose beta regression for analysing the relative abundance of EMF, AMF and NFB as a function of the underlying plot-level abiotic factors. Beta regression allowed us to evaluate the relative abundance of each strategy as a continuous variable bounded by 0 and 1, as it takes into account the error structure of proportional data. To account for the presence of 0 and 1 values in our dataset, we used a standard[52] transformation ($y \times (n-1) + 0.5)/n$), where y is the abundance in each plot and n is the total number of plots in the analysis. The beta regression evaluates two parameters[53]—the population mean (μ) and dispersion (ϕ)—and we fitted the explanatory abiotic factors sequentially to (1) increase the model log-likelihood value and (2) decrease the Bayesian information criterion value.

ϕ takes on values from 0 to infinity, with $\phi > 1$ indicating a centralized single-peak distribution and $\phi < 1$ indicating a bimodal distribution (Supplementary Fig. 7).

For each FIA plot in our analysis ($n = 6{,}159$), we predicted population statistics (μ and ϕ) for either EMF (shown in Fig. 5) or AMF (Supplementary Fig. 5), based on the observed plot-level abiotic factors. Next, we classified each plot as probably drawn from an AMF–EMF bistable population if: (1) neither EMF nor AMF dominated the population (that is, $0.3 < \mu < 0.7$ for either strategy); and (2) the overall population dispersion was bimodal (that is, $\phi < 1$). The resulting plots and bimodal distributions are labelled red in Fig. 5a and Supplementary Fig. 5.

Plot-level simulation of community composition. We used our model to predict the symbiotic composition across all plots in the Gentry dataset ($n = 225$) and a subset of plots in the FIA database ($n = 6{,}159$). Since both mineralization (m) and disturbance (d) vary with latitude in our general model, we approximated both factors based on plot-level mean annual temperature, and assuming a Q_{10} temperature sensitivity coefficient of 1.2 (Supplementary Note 8). We further assumed that plots that were not subject to glaciation during the Last Glacial Maximum had low rates of weathering phosphorous input, while glaciated plots had high rates (Table 1).

To evaluate the probabilistic distribution of community composition, and to mimic the real-world dynamics of plant community succession, we allowed our model to be influenced by disturbance as a stochastic factor. Specifically, we used simulation from a single patch to predict the community composition of each real-world plot. This approach differs from our Fig. 3a biome-level analysis in which mean values were derived from 400 simulation patches. For the FIA dataset, we evaluated a single prediction from each plot, while for the Gentry dataset we replicated each plot in our analysis 10 times due to the small sample size of plots in some biomes (for example, $n = 3$ for the boreal biome).

Global land biosphere properties. We derived the emergent properties of Table 1 as follows: (1) we modelled each biome as described in the section 'Landscape dynamics analysis'; (2) each biome was defined by the biome-specific variables G, m, I_p and d (Table 1 and Supplementary Table 1); (3) we quantified emergent properties once the model reached a state of dynamic equilibrium. We calculated the carbon, nitrogen and phosphorus properties of each biome as the average across all 400 landscape patches. Nitrogen deposition input was held constant across all biomes at a value that can be considered unpolluted. We assumed that nitrogen losses from disturbed landscape patches were equally distributed across dissolved organic (1/3), dissolved inorganic (1/3) and gaseous (1/3) loss vectors. In undisturbed patches, we assumed that gaseous nitrogen loss (N_2 and N_2O) was one-third of the observed inorganic loss. We calculated soil carbon from biome-specific carbon-to-nitrogen ratios derived from a global dataset ($n = 1{,}848$ across boreal, temperate and tropical forests[5]).

Statistics. We used linear regression to test the relationship between the relative fixer abundance versus the strength of phosphorus limitation across simulated forest patches in both temperate and tropical biomes. The model distributions of both fixer abundance and phosphorus limitation strength were skewed to the right, and were corrected to normality using square root transformation. We used beta regression (R package 'betareg'[74]) to: (1) examine the significance of latitudinal trends in the Gentry field data; and (2) detect bistability in the FIA dataset, as detailed above. All significance levels were from two-sided tests. All statistical analyses were performed using the R platform (R version 3.4.1).

Reporting Summary. Further information on research design is available in the Nature Research Reporting Summary linked to this article.

Code availability. The R scripts used in Fig. 2 and MATLAB scripts used in Figs. 3–5 and Table 1 are available from the corresponding author upon reasonable request.

Data availability

The data that support the findings of this study are available from the corresponding author upon reasonable request.

Received: 19 June 2018; Accepted: 20 November 2018;
Published online: 21 January 2019

References

1. Read, D. J. in *The Ecology and Physiology of the Fungal Mycelium* (eds Jennings, D. H. & Yayner, A. M. D.) 215–240 (Cambridge Univ. Press, New York, 1984).
2. Smith, S. E. & Read, D. J. *Mycorrhizal Symbiosis* 3rd edn (Elsevier Science, Academic press, 2008).
3. Lambers, H., Raven, J. A., Shaver, G. R. & Smith, S. E. Plant nutrient-acquisition strategies change with soil age. *Trends Ecol. Evol.* **23**, 95–103 (2008).
4. Bennett, J. A. et al. Plant–soil feedbacks and mycorrhizal type influence temperate forest population dynamics. *Science* **355**, 181–184 (2017).
5. Sheffer, E., Batterman, S. A., Levin, S. A. & Hedin, L. O. Biome-scale nitrogen fixation strategies selected by climatic constraints on nitrogen cycle. *Nat. Plants* **1**, 15182 (2015).
6. Houlton, B. Z., Wang, Y. P., Vitousek, P. M. & Field, C. B. A unifying framework for dinitrogen fixation in the terrestrial biosphere. *Nature* **454**, 327–334 (2008).
7. Batterman, S. A. et al. Key role of symbiotic dinitrogen fixation in tropical forest secondary succession. *Nature* **502**, 224–227 (2013).
8. Averill, C., Turner, B. L. & Finzi, A. C. Mycorrhiza-mediated competition between plants and decomposers drives soil carbon storage. *Nature* **505**, 543–545 (2014).
9. Terrer, C., Vicca, S., Hungate, B. A., Phillips, R. P. & Prentice, I. C. Mycorrhizal association as a primary control of the CO_2 fertilization effect. *Science* **353**, 72–74 (2016).
10. Hedin, L. O., Brookshire, E. N. J., Menge, D. N. L. & Barron, A. R. The nitrogen paradox in tropical forest ecosystems. *Annu. Rev. Ecol. Evol. Syst.* **40**, 613–635 (2009).
11. Smith, S. E. & Smith, F. A. Roles of arbuscular mycorrhizas in plant nutrition and growth: new paradigms from cellular to ecosystem scales. *Annu. Rev. Plant Biol.* **62**, 227–250 (2011).
12. Talbot, J. M., Allison, S. D. & Treseder, K. K. Decomposers in disguise: mycorrhizal fungi as regulators of soil C dynamics in ecosystems under global change. *Funct. Ecol.* **22**, 955–963 (2008).
13. McGuire, K. L., Zak, D. R., Edwards, I. P., Blackwood, C. B. & Upchurch, R. Slowed decomposition is biotically mediated in an ectomycorrhizal, tropical rain forest. *Oecologia* **164**, 785–795 (2010).
14. Sprent, J. *Legume Nodulation: a Global Perspective* (John Wiley & Sons, Wiley-Blackwell, 2009).
15. Ma, Z. et al. Evolutionary history resolves global organization of root functional traits. *Nature* **555**, 94–97 (2018).
16. Cairney, J. W. G. Evolution of mycorrhiza systems. *Naturwissenschaften* **87**, 467–475 (2000).
17. Brundrett, M. C. Coevolution of roots and mycorrhizas of land plants. *New Phytol.* **154**, 275–304 (2002).
18. Tedersoo, L., May, T. W. & Smith, M. E. Ectomycorrhizal lifestyle in fungi: global diversity, distribution, and evolution of phylogenetic lineages. *Mycorrhiza* **20**, 217–263 (2010).
19. Werner, G. D., Cornwell, W. K., Cornelissen, J. H. & Kiers, E. T. Evolutionary signals of symbiotic persistence in the legume–rhizobia mutualism. *Proc. Natl Acad. Sci. USA* **112**, 10262–10269 (2015).
20. Jenny, H. Causes of the high nitrogen and organic matter content of certain tropical forest soils. *Soil Sci.* **69**, 63–69 (1950).
21. Peh, K. S. H., Lewis, S. L. & Lloyd, J. Mechanisms of monodominance in diverse tropical tree-dominated systems. *J. Ecol.* **99**, 891–898 (2011).
22. Peay, K. G., Kennedy, P. G., Davies, S. J., Tan, S. & Bruns, T. D. Potential link between plant and fungal distributions in a dipterocarp rainforest: community and phylogenetic structure of tropical ectomycorrhizal fungi across a plant and soil ecotone. *New Phytol.* **185**, 529–542 (2010).
23. Barron, A. R., Purves, D. W. & Hedin, L. O. Facultative nitrogen fixation by canopy legumes in a lowland tropical forest. *Oecologia* **165**, 511–520 (2011).
24. Bauters, M., Mapenzi, N., Kearsley, E., Vanlauwe, B. & Boeckx, P. Facultative nitrogen fixation by legumes in the central Congo basin is downregulated during late successional stages. *Biotropica* **48**, 281–284 (2016).
25. Menge, D. N. L. & Hedin, L. O. Nitrogen fixation in different biogeochemical niches along a 120 000-year chronosequence in New Zealand. *Ecology* **90**, 2190–2201 (2009).
26. Stephenson, N. L. & van Mantgem, P. J. Forest turnover rates follow global and regional patterns of productivity. *Ecol. Lett.* **8**, 524–531 (2005).
27. Fay, P. A. et al. Grassland productivity limited by multiple nutrients. *Nat. Plants* **1**, 15080 (2015).
28. Davidson, E. A. et al. Nitrogen and phosphorus limitation of biomass growth in a tropical secondary forest. *Ecol. Appl.* **14**, 150–163 (2004).
29. Batterman, S. A., Wurzburger, N. & Hedin, L. O. Nitrogen and phosphorus interact to control tropical symbiotic N_2 fixation: a test in *Inga punctata*. *J. Ecol.* **101**, 1400–1408 (2013).
30. Gökkaya, K., Hurd, T. M. & Raynal, D. J. Symbiont nitrogenase, alder growth, and soil nitrate response to phosphorus addition in alder (*Alnus incana* ssp. *rugosa*) wetlands of the Adirondack Mountains, New York State, USA. *Environ. Exp. Bot.* **55**, 97–109 (2006).
31. Uliassi, D. D. & Ruess, R. W. Limitations to symbiotic nitrogen fixation in primary succession on the Tanana River floodplain. *Ecology* **83**, 88–103 (2002).
32. Vitousek, P. M. & Farrington, H. Nutrient limitation and soil development: experimental test of a biogeochemical theory. *Biogeochemistry* **37**, 63–75 (1997).
33. Connell, J. H. & Lowman, M. D. Low-diversity tropical rain forests: some possible mechanisms for their existence. *Am. Nat.* **134**, 88–119 (1989).
34. Phillips, R. P., Brzostek, E. & Midgley, M. G. The mycorrhizal-associated nutrient economy: a new framework for predicting carbon–nutrient couplings in temperate forests. *New Phytol.* **199**, 41–51 (2013).

35. Scheffer, M. et al. Early-warning signals for critical transitions. *Nature* **461**, 53–59 (2009).
36. Phillips, O. & Miller, J. S. *Global Patterns of Plant Diversity: Alwyn H. Gentry's Forest Transect Data Set* (Missouri Botanical Press, St. Louis, 2002).
37. Read, D. J. Mycorrhizas in ecosystems. *Experientia* **47**, 376–391 (1991).
38. Read, D. J. & Perez-Moreno, J. Mycorrhizas and nutrient cycling in ecosystems—a journey towards relevance? *New Phytol.* **157**, 475–492 (2003).
39. HussDanell, K. Tansley Review No. 93. Actinorhizal symbioses and their N_2 fixation. *New Phytol.* **136**, 375–405 (1997).
40. Bond, G. in *Biological Nitrogen Fixation in Forest Ecosystems: Foundations and Applications* (eds Gordon, J. C. & Wheeler, C. T.) 55–87 (Martinus Nijhoff Publishers, The Hague, 1983).
41. Racette, S. & Torrey, J. G. The isolation, culture and infectivity of a *Frankia* strain from *Gymnostoma papuanum* (Casuarinaceae). *Plant Soil* **118**, 165–170 (1989).
42. Pawlowski, K. & Newton, W. E. *Nitrogen-Fixing Actinorhizal Symbioses* (Springer, Dordrecht, 2008).
43. Wang, B. & Qiu, Y. L. Phylogenetic distribution and evolution of mycorrhizas in land plants. *Mycorrhiza* **16**, 299–363 (2006).
44. Brundrett, M. Mycorrhizas in natural ecosystems. *Adv. Ecol. Res.* **21**, 171–313 (1991).
45. Beer, C. et al. Terrestrial gross carbon dioxide uptake: global distribution and covariation with climate. *Science* **329**, 834–838 (2010).
46. Manzoni, S., Trofymow, J. A., Jackson, R. B. & Porporato, A. Stoichiometric controls on carbon, nitrogen, and phosphorus dynamics in decomposing litter. *Ecol. Monogr.* **80**, 89–106 (2010).
47. Lin, G. G., McCormack, M. L., Ma, C. E. & Guo, D. L. Similar below-ground carbon cycling dynamics but contrasting modes of nitrogen cycling between arbuscular mycorrhizal and ectomycorrhizal forests. *New Phytol.* **213**, 1440–1451 (2017).
48. Barron, A. R. et al. Molybdenum limitation of asymbiotic nitrogen fixation in tropical forest soils. *Nat. Geosci.* **2**, 42–45 (2009).
49. Binkley, D., Sollins, P., Bell, R., Sachs, D. & Myrold, D. Biogeochemistry of adjacent conifer and alder-conifer stands. *Ecology* **73**, 2022–2033 (1992).
50. Fick, S. E. & Hijmans, R. J. WorldClim 2: new 1-km spatial resolution climate surfaces for global land areas. *Int. J. Climatol.* **37**, 4302–4315 (2017).
51. Fischer, G. et al. *Global Agro-ecological Zones Assessment for Agriculture (GAEZ 2008)* (IIASA & FAO, 2008).
52. Smithson, M. & Verkuilen, J. A better lemon squeezer? Maximum-likelihood regression with beta-distributed dependent variables. *Psychol. Methods* **11**, 54–71 (2006).
53. Bayer, F. M. & Cribari-Neto, F. Model selection criteria in beta regression with varying dispersion. *Commun. Stat. Simul. Comput.* **46**, 729–746 (2017).
54. Cribari-Neto, F. & Zeileis, A. Beta regression in R. *J. Appl. Stat.* **34**, 1–24 (2010).
55. Pan, Y. D., Birdsey, R. A., Phillips, O. L. & Jackson, R. B. The structure, distribution, and biomass of the world's forests. *Annu. Rev. Ecol. Evol. Syst.* **44**, 593–622 (2013).
56. Vitousek, P. & Sanford, R. Nutrient cycling in moist tropical forest. *Annu. Rev. Ecol. Syst.* **17**, 137–167 (1986).
57. Menge, D. N. L., Lichstein, J. W. & Angeles-Perez, G. Nitrogen fixation strategies can explain the latitudinal shift in nitrogen-fixing tree abundance. *Ecology* **95**, 2236–2245 (2014).
58. Ter Steege, H. et al. Continental-scale patterns of canopy tree composition and function across Amazonia. *Nature* **443**, 444–447 (2006).
59. Reich, P. B., Grigal, D. F., Aber, J. D. & Gower, S. T. Nitrogen mineralization and productivity in 50 hardwood and conifer stands on diverse soils. *Ecology* **78**, 335–347 (1997).
60. Cleveland, C. C. et al. Global patterns of terrestrial biological nitrogen (N_2) fixation in natural ecosystems. *Glob. Biogeochem. Cycles* **13**, 623–645 (1999).
61. Sullivan, B. W. et al. Spatially robust estimates of biological nitrogen (N) fixation imply substantial human alteration of the tropical N cycle. *Proc. Natl Acad. Sci. USA* **111**, 8101–8106 (2014).
62. Hedin, L. O., Armesto, J. J. & Johnson, A. H. Patterns of nutrient loss from unpolluted, old-growth temperate forests—evaluation of biogeochemical theory. *Ecology* **76**, 493–509 (1995).
63. Brookshire, E. N. J., Hedin, L. O., Newbold, J. D., Sigman, D. M. & Jackson, J. K. Sustained losses of bioavailable nitrogen from montane tropical forests. *Nat. Geosci.* **5**, 123–126 (2012).
64. Bai, E., Houlton, B. Z. & Wang, Y. P. Isotopic identification of nitrogen hotspots across natural terrestrial ecosystems. *Biogeosciences* **9**, 3287–3304 (2012).
65. Fang, Y. T. et al. Microbial denitrification dominates nitrate losses from forest ecosystems. *Proc. Natl Acad. Sci. USA* **112**, 1470–1474 (2015).
66. Houlton, B. Z., Sigman, D. M. & Hedin, L. O. Isotopic evidence for large gaseous nitrogen losses from tropical rainforests. *Proc. Natl Acad. Sci. USA* **103**, 8745–8750 (2006).
67. Hedin, L. O., Vitousek, P. M. & Matson, P. A. Nutrient losses over four million years of tropical forest development. *Ecology* **84**, 2231–2255 (2003).
68. Lewis, W. M., Melack, J. M., McDowell, W. H., McClain, M. & Richey, J. E. Nitrogen yields from undisturbed watersheds in the Americas. *Biogeochemistry* **46**, 149–162 (1999).
69. Hao, S., Xue, J., Guo, D. & Wang, D. Earliest rooting system and root:shoot ratio from a new *Zosterophyllum* plant. *New Phytol.* **185**, 217–225 (2010).
70. Strullu-Derrien, C. et al. Fungal associations in *Horneophyton ligneri* from the Rhynie Chert (c. 407 million year old) closely resemble those in extant lower land plants: novel insights into ancestral plant–fungus symbioses. *New Phytol.* **203**, 964–979 (2014).
71. Bonfante, P. & Genre, A. Mechanisms underlying beneficial plant–fungus interactions in mycorrhizal symbiosis. *Nat. Commun.* **1**, 48 (2010).
72. Henkel, T. W. Monodominance in the ectomycorrhizal *Dicymbe corymbosa* (Caesalpiniaceae) from Guyana. *J. Trop. Ecol.* **19**, 417–437 (2003).
73. Makana, J. R. et al. Demography and biomass change in monodominant and mixed old-growth forest of the Congo. *J. Trop. Ecol.* **27**, 447–461 (2011).
74. Hayman, D. Mycorrhizae of nitrogen-fixing legumes. *MIRCEN J. Appl. Microbiol. Biotechnol.* **2**, 121–145 (1986).
75. McGroddy, M. E., Daufresne, T. & Hedin, L. O. Scaling of C:N:P stoichiometry in forests worldwide: implications of terrestrial redfield-type ratios. *Ecology* **85**, 2390–2401 (2004).
76. Güsewell, S. N. P ratios in terrestrial plants: variation and functional significance. *New Phytol.* **164**, 243–266 (2004).
77. Vitousek, P. M., Matson, P. A. & Vancleve, K. Nitrogen availability and nitrification during succession—primary, secondary, and old-field seres. *Plant Soil* **115**, 229–239 (1989).
78. Manzoni, S., Jackson, R. B., Trofymow, J. A. & Porporato, A. The global stoichiometry of litter nitrogen mineralization. *Science* **321**, 684–686 (2008).
79. Overpeck, J. T., Rind, D. & Goldberg, R. Climate-induced changes in forest disturbance and vegetation. *Nature* **343**, 51–53 (1990).

Acknowledgements

We thank S. Levin, D. Guo, N. Wurzburger, E. Sheffer and members of the Hedin laboratory for helpful comments, J. Sprent for sharing the nodulation database, Y. L. Qiu for sharing the mycorrhizal database, J. Lichstein and W. Liao for sharing the FIA database, Y. Sun for assisting with artwork and S. Wang for assisting with database compilation. We thank A. H. Gentry, the Missouri Botanical Garden and collectors who assisted A. H. Gentry or contributed data for specific A. H. Gentry sites. This work was supported by grants to L.O.H. from the Dean of Faculty Fund and the Carbon Mitigation Initiative at Princeton University.

Author contributions

M.L. and L.O.H. designed the research. M.L. compiled and analysed the belowground strategies database, performed the modelling work and analysed the output data. M.L. and L.O.H. wrote the paper.

Competing interests

The authors declare no competing interests.

Additional information

Supplementary information is available for this paper at https://doi.org/10.1038/s41559-018-0759-0.

Correspondence and requests for materials should be addressed to M.L.

Reprints and permissions information is available at www.nature.com/reprints.

Publisher's note: Springer Nature remains neutral with regard to jurisdictional claims in published maps and institutional affiliations.